SUPPLEMENTARY INFORMATION

Atomically modulated Cu single-atom catalysts for oxygen reduction reactions towards high power density Zn and Al-air batteries

Nayantara K. Wagh, Sambhaji S. Shinde*, Jung-Ho Lee*

Department of Materials Science and Chemical Engineering, Hanyang University, Ansan, Republic of Korea

List of Contents

1. Supplementary experimental methods

Catalyst fabrication

Chemicals: Copper (II) nitrate trihydrate ($Cu(NO_3)_2 \cdot 3H_2O$), Pyrrole (C_4H_5N), Aniline ($C_6H_5NH_2$), Triton^{TM} X-100 (t-Oct-C6H4-$(OCH_2CH_2)_xOH$, x= 9-10), Ammonium persulfate ($(NH_4)_2S_2O_8$), carbon black, poly(N-vinyl-2-pyrrolidone) (M_W = 40,000), Chloroplatinic acid ($H_2PtCl_6 \cdot 6H_2O$), and Nafion were obtained with the Sigma-Aldrich. Ethanol (C_2H_5OH), acetone, sodium hydroxide (NaOH), potassium hydroxide (KOH), sulfuric acid (H_2SO_4), zinc acetate ($Zn(OAc)_2$), and nitric acid (HNO_3) were attained from Daejung Chemicals. Carbon paper (Spectra carb 2040-A, Fuel Cell Store), Al foil, and Zn plate (Sigma-Aldrich, USA) were used as received. All precursors were used without further purifications. Deionized water was utilized as solvent until otherwise specifically mentioned. Acquired resources were applied further without distillation.

Synthesis of CuSA@CNS catalysts

Triton^{TM} X-100 (TX-100, 60 mg) was dissolved in the deionized water (60 mL) under vigorous stirring for 10 min with the precooled ice bath at 0 ºC, then followed insertion of aniline (380 μL) and pyrrole (290 μL) and kept for 30 min stirring. After that, ammonium persulfate solution (1.9 g in 15 mL deionized water) was transfer in the above suspension and treated over 12 h at the 0 ºC. The hollow carbon-nitrogen nanospheres (CNS) were obtained after multiple washing by deionized water and vacuum drying at 60 ºC for overnight.

Cu single atoms were loaded by mixing obtained CNS (0.5 g) with aqueous copper nitrate trihydrate (100 mg) by ultrasonication for 1 h and then washed by deionized water and vacuum dried for overnight. Finally, the black powder was heat treated for 160 ºC for 1 h under inert atmosphere (N_2) to obtain CuSA@CNS catalysts.

Synthesis of reference Pt/C catalysts

An appropriate amount of $H_2PtCl_6 \cdot 6H_2O$ was reacted with poly(N-vinyl-2-pyrrolidone) (M_W = 40,000) solution under vigorous stirring, followed by the addition of activated carbon. After that, the sodium borohydride ($NaBH_4$) solution was appended to the reaction mixture under stirring for 30 min. Finally, the obtained mixture was collected after centrifugation, several times cleanings with deionized water, and dried at 60 °C for 12 h.

Characterization of the prepared catalysts

Powder X-ray diffraction (PXRD) patterns were measured on Rigaku Smartlab D/max 2500Pc diffractometer with Cu Kα radiation (wavelength of 1.5406 Å). Morphology images were performed by field-emission scanning electron microscopy (FESEM, JEOL-6700F). Transmission electron microscopy (TEM) images were acquired on a Cs-corrected Titan^{TM} 80-300 with an accelerating voltage of 80 kV. Elemental composition maps were recorded by an EDS attached to the SEM/TEM. X-ray photoelectron spectroscopy (XPS) was performed on a VG SCIENTA (R 3000) spectrometer equipped with a monochromatic Al *K*α source.

Electrochemical measurements

The electrochemical performances were performed on an electrochemical workstation (CHI 760 D, CH Instruments) at room temperature with a typical three-electrode electrochemical cell. The Ag/AgCl (with saturated KCl) reference electrode, a graphite rod as the counter electrode, a glassy carbon (GC) rotating disk electrode (RDE, 0.196 cm^2) coated with the catalysts as the working electrode, and 0.1 M aqueous KOH (oxygen-rich) as the electrolyte. The working electrode was fabricated with as-obtained CNS or CuSA@CNS or Pt/C (20 wt%) catalysts placed over the GC using Nafion adhesive (5 wt%, 2 μl) and then dried at room temperature for several hours. Catalysts inks were prepared by dispersing 10 mg of catalysts in the propanol of 1.95 ml and Nafion of 50 μl. Then, 8 μL of the prepared inks were evenly loaded on the GC surface and dried at room temperature. Mass loading for both fabricated catalysts was fixed to be 0.20 mg cm^{-2} for the oxygen reactions. Prior to the measurements, the electrolyte (0.1 M KOH) was saturated by oxygen, and nitrogen flow for 30 min. LSV profiles for oxygen reduction reactions (ORR) were obtained for 1600 rpm with a scan rate of 5 mV s^{-1} in the potential range of 0.2–1.1 V vs. RHE.

Chronoamperometric half-cell reactions durability was evaluated at the respective half-wave potential for ORR. The measured potentials were referenced to the reversible hydrogen electrode (RHE) according to the Nernst equation,

$$E_{RHE} = E_{Ag/Ag/Cl} + 0.059 \times pH + 0.205 \quad \text{(S1)}$$

Performed current densities were also referenced according to the measured geometric surface areas. Electrochemical impedance spectra were obtained for the frequency range of 100 Hz to 1 MHz with a constant bias of 0.05 V. The long-life durability of the catalysts was measured by continuous potentiodynamic sweeps for a scan rate of 100 mV s^{-1}. Mass loading of CuSA@CNS and reference Pt/C catalysts has been placed similarly unless otherwise stated (0.2 mg cm^{-2}).

Oxygen reduction reaction kinetics

The ORR kinetics were evaluated by using different rotational speed LSV profiles. The measured total current density is the sum of the inverse of kinetic current (J_K) and diffusion current (J_d). Every atom or ion on the electrode reacts immediately as the applied overpotential is sufficiently high. The number of oxygen molecules at the electrode surface is almost zero, facilitating a diffusion-limiting plateau. Therefore, the diffusion current is related only to the RDE rotational speeds.

The transferred electron number (n) in oxygen reduction was determined according to the Koutecky–Levich (K–L) equation[S1-S3]:

$$\frac{1}{J} = \frac{1}{J_K} + \frac{1}{B\omega^{1/2}} \quad \text{(S2)}$$

$$B = 0.2nF(D_{O_2})^{2/3}\nu^{-1/6}C_{O_2} \quad \text{(S3)}$$

where B represents the Levich slope, J_K represents the kinetic current, J represents the measured total current, ω represents the electrode rotation rate, n represents the number of electrons transferred for each oxygen molecule, F represents the Faraday constant (F = 96485 C mol^{-1}), D_{O2} represents the O_2 diffusion coefficient in 0.1 M KOH (D_{O2} = 1.9 × 10^{-5} cm^2 s^{-1}), ν represents the kinetic viscosity (0.01 cm^2 s^{-1}) and C_{O2} represents the concentration of O_2 (C_{O2} = 1.2 × 10^{-6} mol cm^{-3}). The considered rotation speeds are in rpm, and therefore, the constant factor 0.2 is multiplied. The peroxide species during ORR reactions were determined by measuring the RRDE polarization profiles for the ring potential of 1.3 V *vs.* RHE. Based on the following expressions, the transferred electron number (n) and peroxide (H_2O_2) yield were evaluated as[S4]:

$$n = 4\frac{I_d}{I_d + I_r/N} \quad \text{(S4)}$$

and

$$H_2O^-(\%) = 100\frac{2I_r/N}{I_d + I_r/N} \quad \text{(S5)}$$

where I_r represents the ring current, I_d represents the disk current, and N represents the current collection efficiency of the Pt ring. N was determined to be 0.42.

Fabrication of Zn-air batteries (ZABs)

Zn–air batteries

The alkaline ZABs were analyzed using the home-constructed electrochemical cells. Air cathodes were constructed by uniform mixing of CuSA@CNS catalysts, carbon black, and nafion (8:1:1) and carbon paper was utilized as current collectors. Further, for comparison, Pt/C catalyst slurry was fabricated by mixing carbon black, polytetrafluoroethylene, and the Pt/C catalysts (1:1:8 w/w) in ethanol/Nafion solution. The mass loadings of the CuSA@CNS and reference Pt/C catalysts for alkaline ZABs was 2 mg cm^{-2}. Here, 6 M KOH with 0.2 M zinc acetate was used as the liquid electrolyte for the reversible electrochemical reactions. Catalyst-loaded (Pt/C or CuSA@CNS) carbon paper was used as an air cathode and a polished Zn plate (0.5 mm thickness) as anode.

Al–air batteries

Aluminum-air batteries (AABs) were analyzed using the home-constructed electrochemical cells. Air cathodes were constructed by uniform mixing of CuSA@CNS catalysts, carbon black, and nafion (8:1:1) and carbon paper was utilized as current collectors. Further, for comparison, Pt/C catalyst slurry was fabricated by mixing carbon black, polytetrafluoroethylene, and the Pt/C catalysts (1:1:8 w/w) in ethanol/Nafion solution. The mass loadings of the CuSA@CNS and reference Pt/C catalysts for alkaline AABs was 2 mg cm^{-2}. Here, 3 M KOH with mixture of ethylene glycol/water (1:1 v/v) was used as the liquid electrolyte for the electrochemical reactions. Catalyst-loaded (Pt/C or CuSA@CNS) carbon paper was used as an air cathode and the Al foil (0.3 mm thickness) as anode.

Battery testing

Note all the measurements were carried out in ambient conditions. The specific capacities were determined using the galvanostatic discharge profiles standardized to the utilized mass of Zn and Al for ZABs and AABs, respectively. The power densities of both ZABs and AABs were calculated by considering the equation of $P = V\times I$. The discharge and charge polarizations were conducted on a WONATEC multichannel battery testing system. (Conditions- charge: 5 min; discharge: 5 min for 50 mA cm^{-2}).

Supplementary Figures

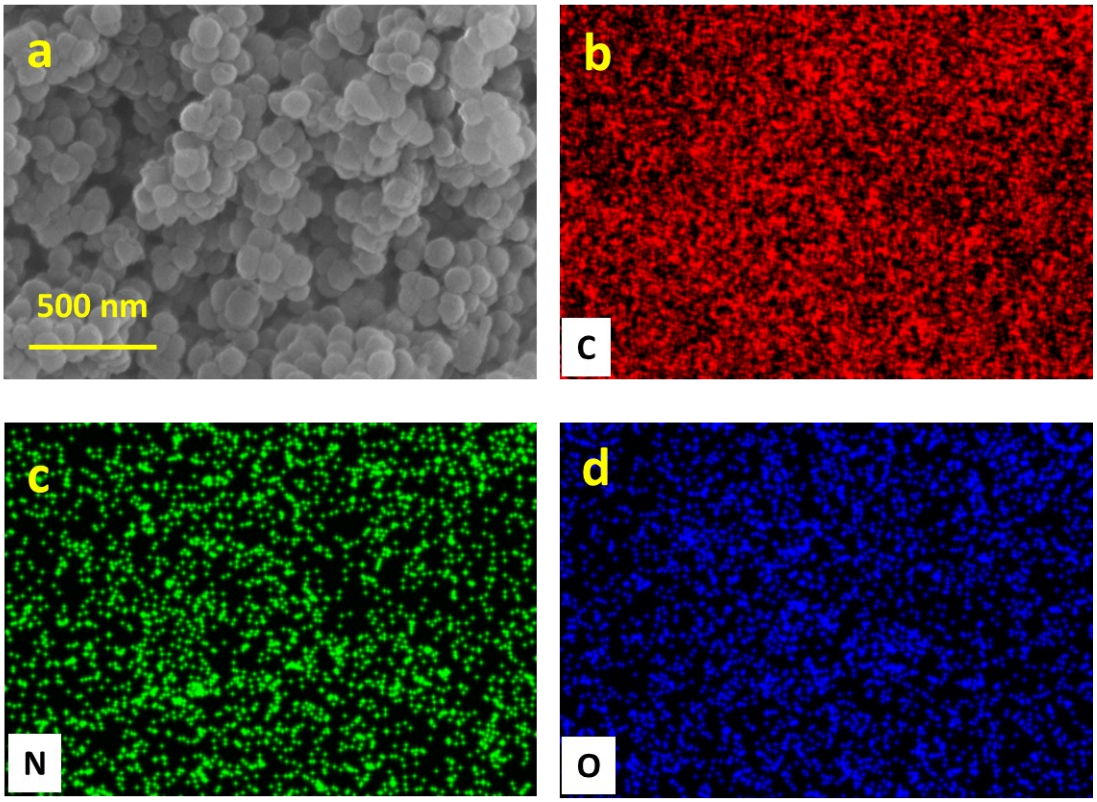

Figure S1. (a) SEM image and (b-d) EDS maps of C, N, O elements for the prepared CNS catalysts.

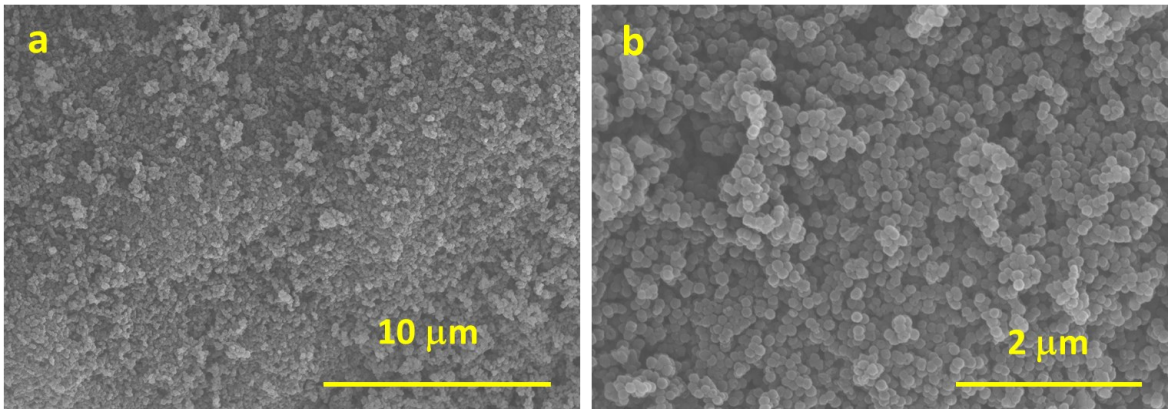

Figure S2. (a-b) SEM images of CuSA@CNS catalysts for 10 and 2 μm scales.

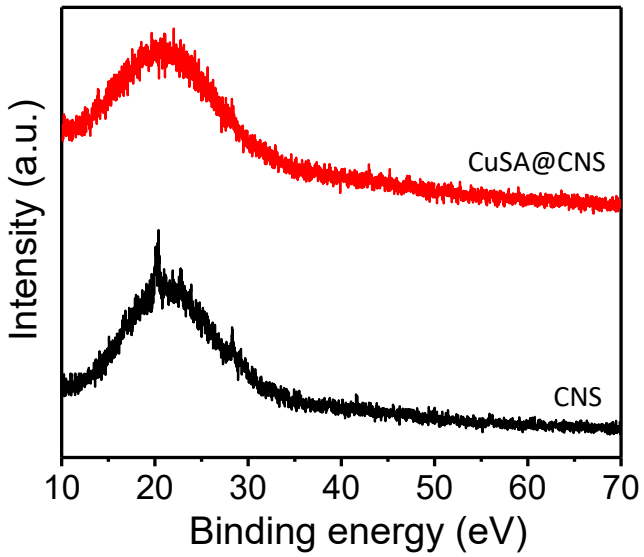

Figure S3. X-ray diffraction patterns of pristine CNS and CuSA@CNS catalysts.

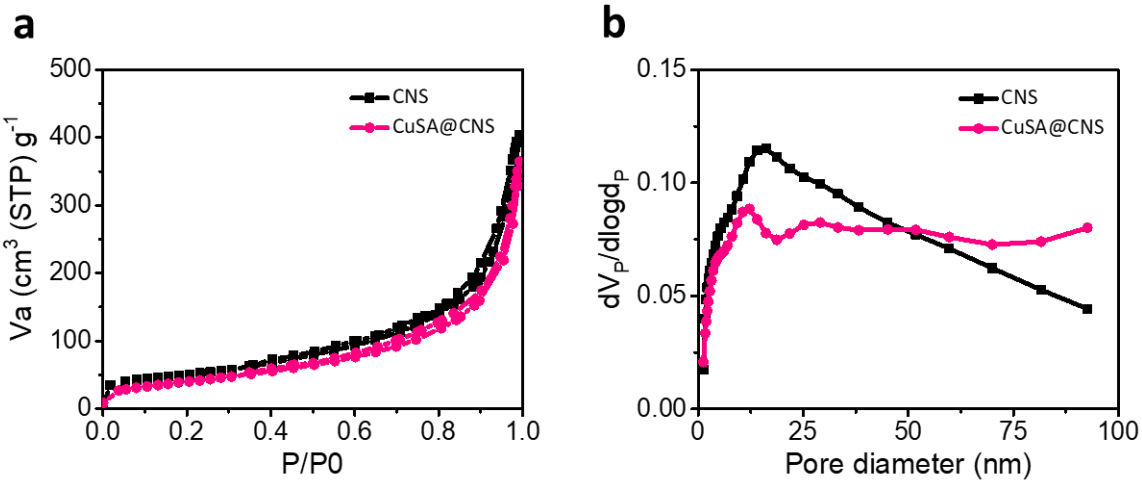

Figure S4. (a) Nitrogen sorptions and (b) pore distributions for CNS and CuSA@CNS catalysts.

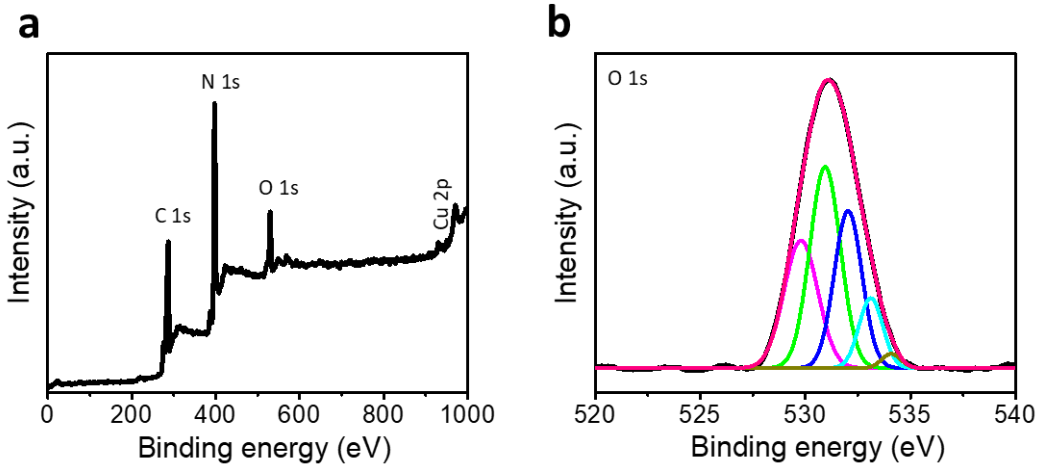

Figure S5. (a) XPS survey scan spectra and (b) high-resolution O 1s spectra for CuSA@CNS catalysts.

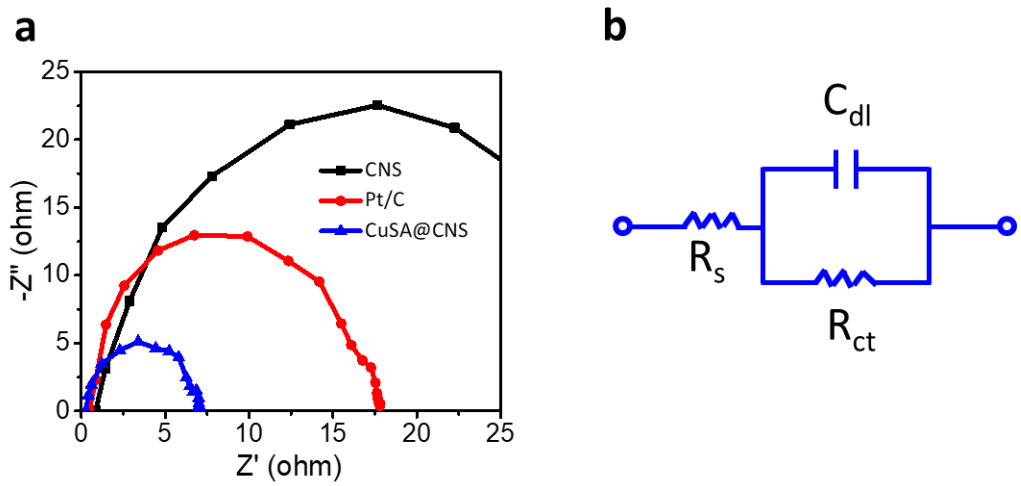

Figure S6. (a) Electrochemical impedance spectra (EIS) for the CNS, Pt/C, and CuSA@CNS catalysts. (b) Equivalent circuit.

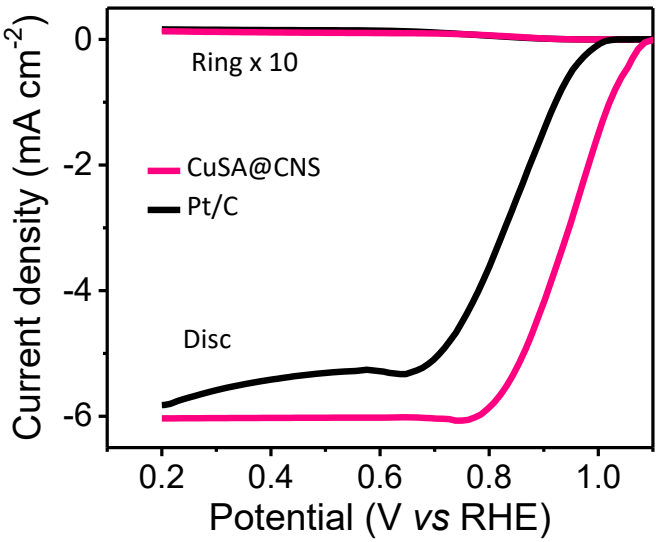

Figure S7. Disc and ring current LSV polarizations for CuSA@CNS and reference Pt/C catalysts.

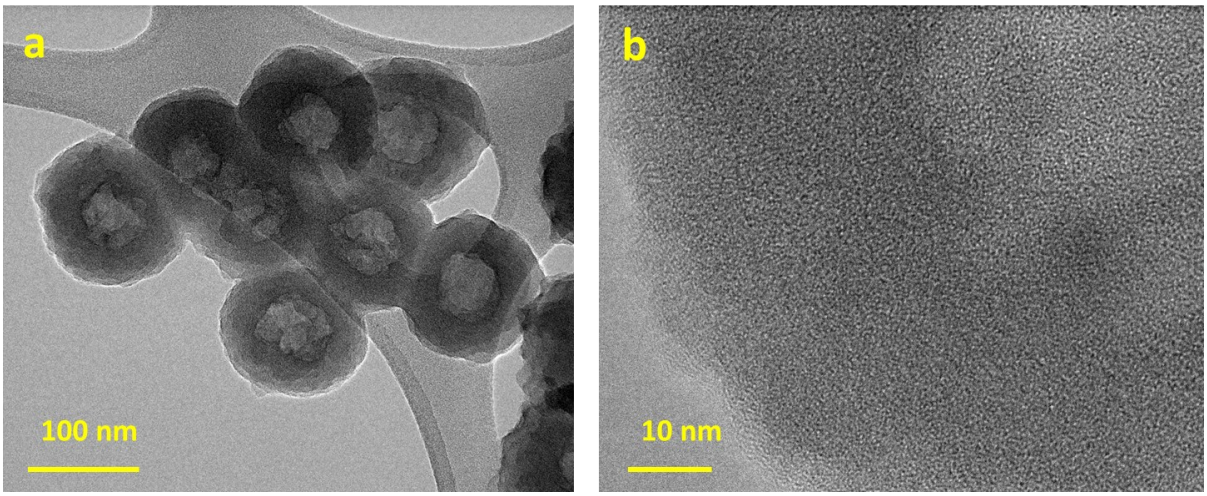

Figure S8. (a) TEM image and (b) HRTEM image of CuSA@CNS after ORR stability tests.

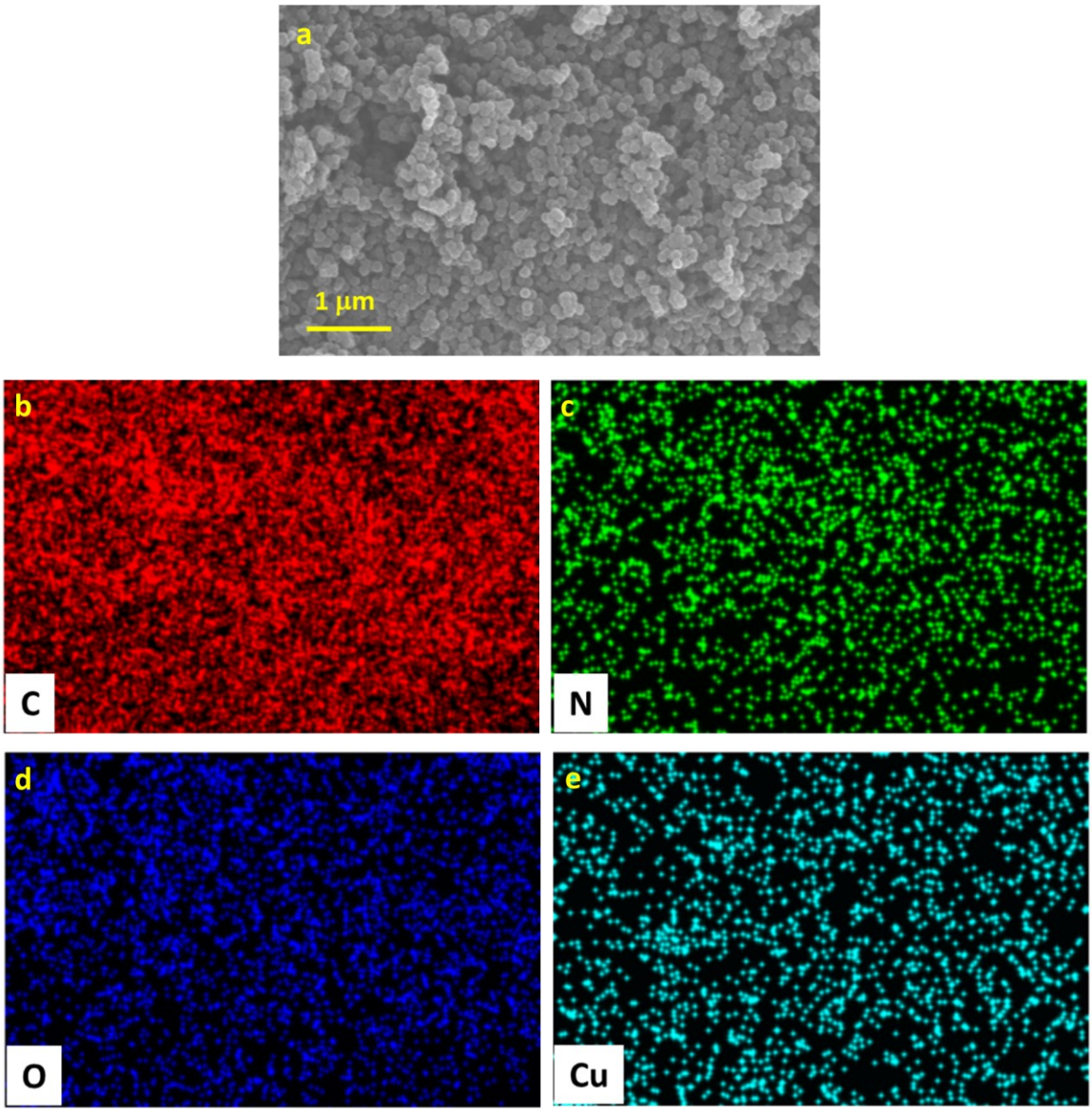

Figure S9. (a) SEM image, and (b) EDS maps of CuSA@CNS after ORR stability.

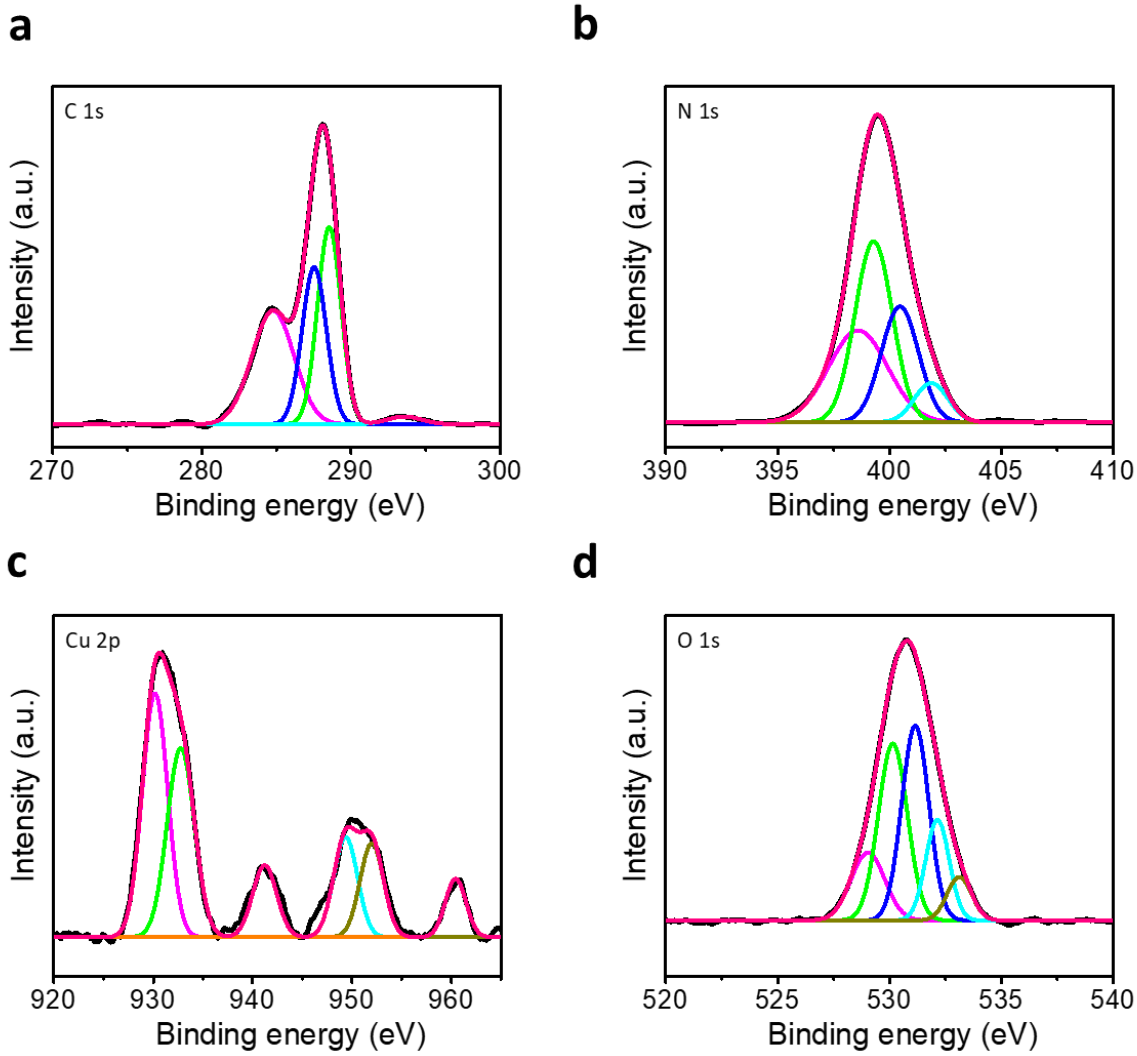

Figure S10. XPS spectra for CuSA@CNS after ORR stability. (a) C 1s, (b) N 1s, (c) Cu 2p, and (d) O 1s.

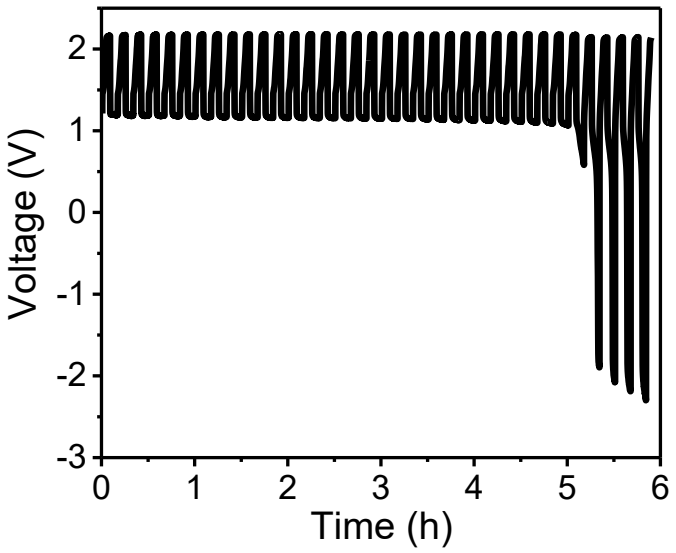

Figure S11. Charge-discharge cycle operations for Pt/C + RuO_2 based aqueous ZABs for 50 mA cm^{-2}.

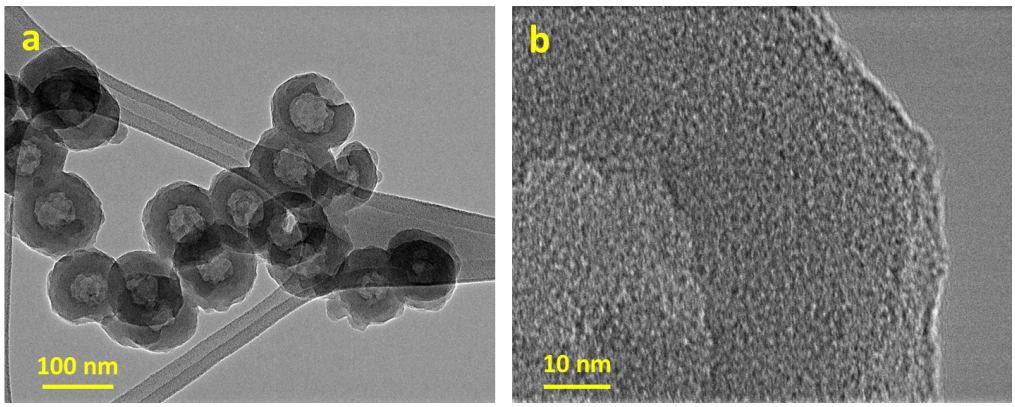

Figure S12. (a) TEM image and (b) HRTEM image of CuSA@CNS after 300 cycles of ZABs at 50 mA cm^{-2}.

Supplementary Tables

Table S1. The elemental stoichiometry distributions of prepared catalysts.

Sample	C (at.%)	N (at.%)	O (at.%)	Cu (at.%)
CNS	63.74	23.93	12.33	-
CuSA@CNS (initial)	62.30	22.94	9.16	5.60
CuSA@CNS (after stability test)	61.16	21.01	13.01	4.82

Table S2. Evaluation of ORR performance for the prepared CuSA@CNS and reported champion catalysts.

Catalyst	Loading (mg cm^{-2})	ORR onset potential (V *vs.* RHE)	ORR Tafel slope (mV dec^{-1})	ORR half-wave potential ($E_{1/2}$) (V *vs.* RHE)	References
CuSA@CNS	0.20	1.09	37	0.95	This work
FeSA@CNS	0.20	1.00	-	0.88	This work
CoSA@CNS	0.20	0.82	-	0.70	This work
NiSA@CNS	0.20	0.78	-	0.65	This work
MnSA@CNS	0.20	0.81	-	0.69	This work
NDC-800	-	1.03	79.53	0.88	S5
Co_4N/PNC-920	-	-	56	0.86	S6
CoFe-FeNC	-	1.12	80.83	0.876	S7
FeCo@NC-II	-	0.999	61.5	0.91	S8
Co_{SA}Ni-NCNT/CNF	-	0.91	58	0.86	S9
$CoS_{1-\delta}/SnS_{2-\delta}$	0.10	-	46	0.90	S10
PEMAC@NDCN	0.15	-	42	0.87	S11
Mn/Fe-HIB-MOF	0.15	0.98	36	0.883	S12
Fe/SNCFs-NH_3	-	-	70.82	0.89	S13

CPS(101)	0.1	0.99	39	0.90	S14
FeCo SAs@Co/N-GC	0.25	0.98	49	0.88	S15
Ni SAs-NC	0.1	-	-	0.85	S16
Co@IC/MoC@PC	0.4	-	78	0.875	S17
PS-CNS	0.15	0.97	61	0.87	S18
1100-CNS	0.42	0.99	58	0.88	S19
S-C_2NA	0.15	0.98	54	0.88	S20
FeN_x-PNC	0.14	0.99	-	0.86	S21
Co/Co_3O_4@PGS	0.3	0.97	52.6	0.89	S22
FeNi@N-GR	0.2	0.94	-	0.83	S23
PS-CNF	0.2	0.95	29	0.86	S24
S,N-Fe/N/C-CNT	0.25	0.94	-	0.84	S25
N-GCNT/FeCo-3	0.40	1.03	66.8	0.92	S26
Ir@Co_3O_4	0.5	-	-	0.75	S27
Co-FPOH	0.283	0.82	183	0.69	S28
Co_4N/CNW/CC	0.20	0.89	-	0.80	S29
NiO/CoN PINWs	0.20	0.89	35	0.68	S30
Re-SAC	-	1.00	72	0.89	S31

Fe/I-N-CR	-	1.025	52.9	0.915	S32
Fe SAs@S/N-C	0.5	0.96	44	0.84	S33
Co-N-B-C	-	0.94	-	0.81	S34
FeNC-V_N	-	0.99	55	0.902	S35
FeSA-FeAC/NC	-	-	73	0.886	S36
FeSA-N/TC	-	-	-	0.925	S37
f-Fe_1Co_1/CNT	0.597	-	35.8	0.88	S38
FeCu SACs@NSC	0.8	-	66.27	0.89	S39
Fe-N/O-C	-	-	73.55	0.927	S40

Table S3. State-of-the-art of CuSA@CNS based ZABs performance in the alkaline electrolytes compared to those of reported superior cathodes.

Catalyst	OCP (V)	Power density (mW cm^{-2})	Specific capacity (mAh g^{-1})	Energy density (Wh kg^{-1})	Durability, h (cycles)@mA cm^{-2}	References
CuSA@CNS	1.57	371	783@20 mA cm^{-2}	1080@20 mA cm^{-2}	53 h (318)@50	This work
NDC-800	-	186.12	630	-	60h (120)@10	S5
Co_4N/PNC-920	1.46	170.7	801.1	-	266h (800)@2	S6
CoFe-FeNC	1.447	120.8	767.5	-	1200@10	S7
FeCo@NC-II	-	212.4	-	1060	150@10	S8
Co_{SA}Ni-NCNT/CNF	1.54	132.23	803.5	-	120@10	S9
$CoS_{1-\delta}/SnS_{2-\delta}$	1.53	249	814	1066	168h (1008)@20	S10
PEMAC@NDCN	1.51	214	817	1070	360h (2160)@20	S11
Pt/C +RuO_2	1.5	178	773	966	-	S11
Mn/Fe-HIB-MOFs	1.50	195	768	1027	1000h (6000)@10	S12
Fe/SNCFs-NH_3	-	255	-	-	1000h (1000)@1	S13
FeCo SAs@Co/N-GC	-	207	741	934	200h (1200)@10	S15
P,S-CNS	1.51	198	830	-	100h (500)@2	S18
S-C_2NA	1.49	209	863	958	750h (375)@10	S20
FeNx-PNC	1.55	278	-	-	40h (220)@5	S21
FeNi@N-GR	1.48	85	765	920	40h (120)@20	S23

PS-CNF	1.49	231	698	907	120h (600)@2	S24
Co-FPOH	-	167.8	817	980	450h (1200)@5	S28
Co_4N/CNW/CC	1.40	174	774	944	136h (408)@10	S29
PFN PF	-	175	816	938	500h (1000)@20	S41
Co_9S_8@N,S-C	-	259	862	-	110h (660)@1	S42
FeCo/Se-CNT	-	175	750	894	70h (210)@5	S43
Co-TMPyP/CCG	-	225	793	-	100h (300)@2	S44
S-GNS/$NiCo_2S_4$	1.38	216.3	-	-	100h (150)@10	S45
CNT@POF	1.49	237	772.7	-	67h (200)@2	S46
CoO/N-CNT	1.40	265	570	-	200h (10)@20	S47
CuPt-NC	1.50	250	560	-	-	S48
MnO_x/C	1.40	190	290	-	-	S49
CuS/NiS_2	1.44	172.4	775	-	83h (500)@25	S50

Table S4. State-of-the-art of CuSA@CNS based AABs performance in the alkaline electrolytes compared to those of reported cathodes.

Catalyst	OCP (V)	Power density (mW cm^{-2})	Specific capacity (mAh g^{-1})	Energy density (Wh kg^{-1})	References
CuSA@CNS	1.79	289	2494@5 mA cm^{-2}	4290@5 mA cm^{-2}	This work
Mn_xO_y@Ag	1.75	172.4	2324	3101@5 mA cm^{-2}	S51
Mn_xO_y@Ag	1.82	-	2096	2913.44	S52
Pt/C	0.98	28	1785	1752	S53
Mn_xO_y	1.45	-	2271	3106	S54
Mn_xO_y@Ag	1.77	-	2324	436.1@system-level	S55
Mn_xO_y	1.5	-	1902	2149	S56

Supplementary References

S1 Y. Liang, H. Wang, J. Zhou, Y. Li, J. Wang, T. Regier, H. Dai, *J. Am. Chem. Soc.,* 2012, **134,** 3517–3523.

S2 Paulus, U. Schmidt, T. and Gasteiger, H. R. Behm, *J. Electroanal. Chem.,* 2001, **495,** 134.

S3 S. Zecevic, J. Wainright, M. Litt, S. Gojkovic, R. Savinell, J. Electrochem. Soc., 1997, **144,** 2973–2982.

S4 O. Antoine, R. Durand, *J. Appl. Electrochem.,* 2000, **30,** 839–844.

S5 P. Li, J. Wen, Y. Xiang , M. Li, Y. Zhao, S. Wang, J. Dou, Y. Li, H. Ma, and L. Xu, *Inorg. Chem. Front.*, 2024, **11**, 5345-5358.

S6 B. Li, Y. Ren, G. Zhang, C. Lv, L. Li, X. Yang, Z.0Lu, X.0Zhang, X. Yu, *Appl. Surface Sci.*, 2025, 161212.

S7 S. Zhang, J. Yang, L. Yang, T. Yang, Y. Liu, L. Zhou, Z. Xu, X. Zhou, J. Tang, *Appl. Catal. B: Environ.*, 2024, **359**, 124485.

S8 Q. Wang, L. Wang, S. Zhang, Z. Chen, W. Peng, Y. Li, X. Fan, *J. Coll. Inter. Sci.*, 2025**, 677**, 800–811.

S9 M. Poudel, M. Balanay, P. Lohani, K. Sekar, and D. Yoo, *Adv. Energy Mater.*, 2024, **14**, 2400347.

S10 N. Wagh, D. Kim, C. Lee, S. Kim, H. Um, J. Kwon, S. Shinde, S. Lee, and J. Lee, *Nanoscale Horiz.,* 2023, **8,** 921-934.

S11 N. Wagh, S. Shinde, C. Lee, S. Kim, D. Kim, H. Um, S. Lee, J. Lee, *Nano-Micro Lett.*, 2022, **14,** 190.

S12 S. Shinde, C. Lee, J. Jung, N. Wagh, S. Kim, D. Kim, C. Lin, S. Lee, J. Lee, *Energy Environ. Sci.*, 2019, **12,** 727-738.

S13 L. Yang, X. Zhang, L. Yu, J. Hou, Z. Zhou, R. Lv, *Adv. Mater.,* 2021, 2105410.

S14 S. Shinde, J. Jung N. Wagh, C. Lee, S. Kim, S. Lee, J. Lee, *Nat. Energy*, 2021, 6, 592-604.

S15 N. Wagh, D. Kim, S. Kim, S. Shinde, J. Lee, *ACS Nano,* 2021, **15,** 14683–14696.

S16 H. Jiang, J. Xia, L. Jiao, X. Meng, P. Wang, C. Lee, W. Zhang, Appl. Catal. B: Environ. **310,** 121352 (2022).

S17 L. Zhang, Y. Zhu, Z. Nie, Z. Li, Y. Ye, L. Li, J. Hong, Z. Bi, Y. Zhou, G. Hu, ACS Nano **15,** 13399−13414 (2021).

S18 Shinde, S.; Lee, C.; Sami, A.; Kim, D.; Lee, S.; Lee, J. ACS Nano 2017, **11,** 347−357.

S19 Pei, Z.; Li, H.; Huang, Y.; Xue, Q.; Huang, Y.; Zhu, M.; Wang, Z.; Zhi, C. Energy Environ. Sci. 2017, **10,** 742-749.

S20 Shinde, S.; Lee, C.; Yu, J.; Kim, D.; Lee, S.; Lee, J. ACS Nano 2018, 12, 596–608.

S21 Ma, L.; Chen, S.; Pei, Z.; Huang, Y.; Liang, G.; Mo, F.; Yang, Q.; Su, J.; Gao, Y.; Zapien, J.; Zhi, C. ACS Nano 2018, 12, 1949−1958.

S22 Jiang, Y.; Deng, Y.; Fu, J.; Lee, D.; Liang, R.; Cano, Z.; Liu, Y.; Bai, Z.; Hwang, S.; Yang, L.; Su, D.; Chu, W.; Chen, Z. Adv. Energy Mater. 2018, 8, 1702900.

S23 Guan, C.; Sumboja, A.; Wu, H.; Ren, W.; Liu, X.; Zhang, H.; Liu, Z.; Cheng, C.; Pennycook, S.; Wang, J. Adv. Mater. 2017, 29, 1704117.

S24 Shinde, S.; Yu, J.; Song, J.; Nam, Y.; Kim, D.; Lee, J. Nanoscale Horiz. 2017, 2, 333-341.

S25 Chen, P.; Zhou, T.; Xing, L.; Xu, K.; Tong, Y.; Xie, H.; Zhang, L.; Yan, W.; Chu, W.; Wu, C.; Xie, Y. Angew. Chem., Int. Ed. 2017, 56, 610–614.

S26 Su, C.; Cheng, H.; Li, W.; Liu, Z.; Li, N.; Hou, Z.; Bai, F.; Zhang, H.; Ma, T. *Adv. Energy Mater.* 2017, **7,** 1602420.

S27 Y. Dai, J. Yu, J. Wang, Z. Shao, D. Guan, Y. Huang, M. Ni, *Adv. Funct. Mater.,* 2022, 2111989.
S28 L. Song, T. Zheng, L. Zheng, B. Lu, H. Chen, Q. He, W. Zheng, Y. Hou, J. Lian, Y. Wu, J. Chen, Z. Ye, J. Lu, *Appl. Catal. B: Environ.,* 2022, **300,** 120712.
S29 Meng, F.; Zhong, H.; Bao, D.; Yan, J.; Zhang X. *J. Am. Chem. Soc.,* 2016, **138,** 10226–10231.
S30 Yin, J.; Li, Y.; Lv, F.; Fan, Q.; Zhao, Y.; Zhang, Q.; Wang, W.; Cheng, F.; Xi, P.; Guo, S. *ACS Nano,* 2017, **11,** 2275−2283.
S31 X. Yue, Y. Liu, B. Lu, X. Du, W. Lei, Z. Liu, S. Yi, and C. Lu, *Energy Environ. Sci.,* 2024, **17,** 5892-5900
S32M. Du, B. Chu, Q. Wang, C. Li, Y. Lu, Z. Zhang, X. Xiao, C. Xu, M. Gu, J. Li, H. Pang, Q. Xu, *Adv. Mater.,* 2024, 2412978.
S33 T. Yang, B. Ge, X. Liu, Z. Zhang, Y. Chen, and Y. Liu, *J. Mater. Chem. A,* 2024, **12,** 11669-11680.
S34 C. Xu, J. Wu, L. Chen, Y. Gong, B. Mao, J. Zhang, J. Deng, M. Mao, Y. Shi, Z. Hou, M. Cao, H. Li, H. Zhou, Z. Huang, Y. Kuang, *Energy Environ. Mater.,* 2024, **7,** e12569.
S35 L. Lyu, X. Hu, S. Lee, W. Fan, G. Kim, J. Zhang, Z. Zhou, Y. Kang, *J. Am. Chem. Soc.,* 2024, **146,** 4803–4813.
S36 P. Rao, Y. Liu, X. Shi, Y. Yu, Y. Zhou, R. Li, Y. Liang, D. Wu, J. Li, X. Tian, Z. Miao, *Adv. Funct. Mater.,* 2024, 2407121.
S37 Y. Yu, Y. Wang, F. Yang, D. Feng, M. Yang, P. Xie, Y. Zhu, M. Shao, Y. Mei, J. Li, *Angew. Chem., Int. Ed.,* 2024, 10.1002/anie.202415691.
S38 Y. Ting, C. Cheng, S. Lin, T. Lin, P. Chen, F. Yen, S. Chang, C. Lee, H. Chen, S. Lu, *Energy Storage Mater.*, 2024, **67,** 103286.
S39 H. Liu, L. Jiang, Y. Liu, B. Lu, L. Li, Y. Tang, Y. Sun, J. Zhou, *Appl. Catal. B: Environ. Energy*, 2025, **362**, 124705.
S40 Y. Li, H. Sun, L. Ren, K. Sun, L. Gao, X. Jin, Q. Xu, W. Liu, X. Sun, *Angew. Chem., Int. Ed.,* 2024, **63,** e202405334.
S41 G. Wang, J. Chang, S. Koul, A. Kushima, Y. Yang, *J. Am. Chem. Soc.,* 2021, **143,** 11595−11601.
S42 D. Lyu, S. Yao, A. Ali, Z. Tian, P. Tsiakaras, P. Shen, *Adv. Energy Mater.*, 2021, **11,** 2101249.
S43 H. Zhang, M. Zhao, H. Liu, S. Shi, Z. Wang, B. Zhang, L. Song, J. Shang, Y. Yang, C. Ma, L. Zheng, Y. Han, W. Huang, *Nano Lett.,* 2021, **21,** 2255−2264.
S44 K. Cui, Q. Wang, Z. Bian, G. Wang, Y. Xu, *Adv. Energy Mater.,* 2021, **11,** 2102062.
S45 Liu, W.; Zhang, J.; Bai, Z.; Jiang, G.; Li, M.; Feng, K.; Yang, L.; Ding, Y.; Yu, T.; Chen, Z.; Yu, A. *Adv. Funct. Mater.,* 2018, **28,** 1706675.
S46 Li, B.; Zhang, S.; Wang, B.; Xia, Z.; Tang, C.; Zhang, Q. *Energy Environ. Sci.,* 2018, **11,** 1723-1729.
S47 Li, Y.; Gong, M.; Liang, Y.; Feng, J.; Kim, J.; Wang, H.; Hong, G.; Zhang, B.; Dai, H. *Nat. Commun.*, 2013, **4,** 1805.
S48 Dhavale, V.; Kurungot, S. *ACS Catal., 2015,* **5,** 1445–1452.
S49 Lee, J.; Park, G.; Lee, H.; Kim, S.; Cao, R.; Liu, M.; Cho, J. *Nano Lett.,* 2011, **11,** 5362–5366.
S50 An, L.; Li, Y.; Luo, M.; Yin, J.; Zhao, Y.; Xu, C.; Cheng, F.; Yang, Y.; Xi, P.; Guo, S. *Adv. Funct. Mater.,* 2017, **27,** 1703779.

S51Y. Xu, Q. Zhao, C. Lv, Y. Zhu, Y. Zhang, F. Peng, Q. Zhao, Z. Peng, Y. Li, Y. Tang, *Energy Storage Mater.,* 2024, 103772. https://doi.org/10.1016/j.ensm.2024.103772.
S52 C. Lv, Y. Li, Y. Zhu, Y. Zhang, J. Kuang, D. Huang, Y. Tang, and H. Wang, *Chem. Eng. J.*, 2023, **462,** 142182.
S53 L. Luo, C. Zhu, L. Yan, L. Guo, Y. Zhou, and B. Xiang, *Chem. Eng. J.*, 2022, **450,** 138175.
S54 T. Wang, Z. Tian, Z. You, Z. Li, H. Cheng, W. Li, Y. Yang, Y. Zhou, Q. Zhong, and Y. Lai, *Energy Storage Mater.*, 2022, **45,** 24-32.
S55 S. Wu, S. Hu, Q. Zhang, D. Sun, P. Wu, Y. Tang, and H. Wang, *Energy Storage Mater.*, 2020, **31,** 310-317.
S56 H. Jiang, S. Yu, W. Li, Y. Yang, L. Yang, and Z. Zhang, *J. Power Sources*, 2020, **448,** 227460.